Steady and Transient Pyrolysis of a Non-charring Solid Fuel Under Forced Flow

Ajay V. Singh[a] and Michael J. Gollner[b]

[a] *Mechanical Engineering Department, Stanford University, Stanford, CA 94305, United States*

[b] *Department of Fire Protection Engineering, University of Maryland, College Park, MD 20742, United States*

Corresponding Author: Michael J. Gollner

Department of Fire Protection Engineering

University of Maryland, College Park

3106 J.M. Patterson Bldg.

College Park, MD 20742, U.S.A.

Email: mgollner@umd.edu

Phone: +1 (301) 405-6667

Fax: +1 (301) 405-9383

Preferred Colloquium: Fire Research

Paper Length: 5596 words (204 available, Method 1)

Text = 3708 words

Equations = 319 words

Equation 1 = (2 lines + 2 blank) × 7.6 words/line × 1 = 30.4

Equation 2 = (2 lines + 2 blank) × 7.6 words/line × 1 = 30.4

Equation 3 = (1 lines + 2 blank) × 7.6 words/line × 1 = 22.8

Equation 4 = (2 lines + 2 blank) × 7.6 words/line × 1 = 30.4

Equation 5 = (2 lines + 2 blank) × 7.6 words/line × 1 = 30.4

Equation 6 = (2 lines + 2 blank) × 7.6 words/line × 1 = 30.4

Equation 7 = (2 lines + 2 blank) × 7.6 words/line × 1 = 30.4

Equation 8 = (2 lines + 2 blank) × 7.6 words/line × 1 = 30.4

Equation 9 = (1 lines + 2 blank) × 7.6 words/line × 1 = 22.8

Equation 10 = (2 lines + 2 blank) × 7.6 words/line × 1 = 30.4

Equation 11 = (2 lines + 2 blank) × 7.6 words/line × 1 = 30.4

References = 262 words

(13+2) × 2.3 × 7.6 = 262

Tables = 289 words

Table 1 = (10+2) × 7.6 × 1 = 91

Table 2 = (11+2) × 7.6 × 2 = 198

Figures and Captions = 1018 words

Figure 1 (58.42 +10) × 2.2 × 1 + 20 = 171

Figure 2 (58.166 +10) × 2.2 × 1 + 17 = 167

Figure 3 (59.182+10) × 2.2 × 1 + 16 = 168

Figure 4 (58.166+10) × 2.2 × 1 + 14 = 164

Figure 5 (62.738+10) × 2.2 × 2 + 28 = 348

Abstract Length: 177 words (123 available)

Color Reproduction: Not Required

Supplemental Material: Attached

Keywords: Reynolds analogy, local pyrolysis rate, local heat fluxes, Nusselt number, PMMA

Steady and Transient Pyrolysis of a Non-charring Solid Fuel Under Forced Flow

Ajay V. Singh[a,*], Michael J. Gollner[b,**]

[a] *Mechanical Engineering Department, Stanford University, Stanford, CA 94305-3032, United States*
[b] *Department of Fire Protection Engineering, University of Maryland, College Park, MD 20742, United States*

Abstract

Reynolds analogy was used earlier to establish a relationship between mass, momentum and heat transfer in a reacting boundary layer over a solid or liquid fuel surface. The relationship was further used to develop a theoretical expression that allowed for the estimation of local mass burning rates in steady laminar boundary layer diffusion flames established over liquid and solid fuels. In order to elucidate mechanisms responsible for the pyrolysis of a solid fuel in a forced convective environment, a thorough experimental investigation of steady and transient pyrolysis of clear cast Poly Methyl Methacrylate (PMMA) was conducted on a bench scale experimental apparatus. Local pyrolysis rates and heat feedback to the condensed fuel surface were measured at different streamwise locations along the fuel surface along with local convective heat transfer coefficients. A functional form of the Nusselt number was derived for boundary layer combustion of a solid fuel. The theoretical formula for the Nusselt number is then presented in a form that can be readily used in applications to identify the steady and transient regimes of PMMA burning.

Keywords: Reynolds analogy, local pyrolysis rate, local heat fluxes, Nusselt number, PMMA

*Postdoctoral scholar, Mechanical Engineering Dept.
**Corresponding author, Assistant Professor, Dept. of Fire Protection Engineering
Email address: mgollner@umd.edu (Michael J. Gollner)

1. Introduction

Diffusion flames in laminar boundary layers have been widely studied mainly because of the importance of this problem in the study of fires and solid propellant burning. This type of diffusion flame also presents a number of characteristics which permit fundamental studies on the mechanism of combustion for liquid and solid fuels. In particular, mathematical modeling of these flames appears to be reasonably simple; temperature and velocity fields can be considered to be monodimensional in terms of the boundary layer coordinate; the length across the flame over which diffusion of species and chemical reactions occurs can be sufficiently large to allow a precise spatial resolution of the flame; these flames are very stable and their characteristics can be kept constant for long times.

Boundary layer diffusion flames have been studied in fire science from the point of view of understanding the flame spread mechanisms in such flames. While critical advancements have been made in the area of fire safety research over the past century, predicting rates of flame spread still remains a challenge for many materials in diverse configurations. The local mass loss (or burning) rate, $\dot{m}''_f$, can be thought of as a measure of the flammability of a material and is a critical parameter in fire risk analysis and the design of fire suppression systems. While knowledge of integrated mass-loss rates are relatively well known, knowledge of mass-burning rates at incremental locations along a fuel surface are not well known because experimental techniques to measure such rates are extremely limited. A technique that provides this local mass-burning rate information for steady flames was developed earlier that provided increased insight to the burning of condensed fuels [1, 2, 3]. In this work, the technique will be extended to unsteady burning of solid fuels and presented with a simple functional form of the Nusselt number, enabling researchers to further understand the mechanisms which distinguish different fuels or configurations from one another. Identifying the steady and transient burning regimes of a solid fuel is also looked upon as a big challenge. This is important in understanding

the mechanisms that affect solid fuel pyrolysis and flame spread rate and constitutes the primary motivation for this work. The present paper is offered as a contribution to this end.

2. Reynolds Analogy

A methodology based on the Reynolds analogy was developed earlier [1, 2, 3] that allowed for the estimation of local mass burning rates in free and forced convective laminar boundary-layer diffusion flames. An expression for local mass burning rate was derived which was given by [2, 3]

$$\dot{m}''_f = \frac{Bk_w}{c_p L}(\mathrm{Pr})^{2/3}\left(\frac{\partial T^*}{\partial y^*}\right)_{y^*=0} = \frac{Bk_w}{c_p L}\left(\frac{\partial T^*}{\partial y^*}\right)_{y^*=0}, \qquad (1)$$

where $T^* = (T - T_{w,p}/T_{fl,ad} - T_{w,p})$ represents the non dimensional temperature, $T_{w,p}$ and $T_{fl,ad}$ represent the wall (taken as the pyrolysis temperature of the given fuel) and adiabatic flame temperature, respectively for a given fuel, L is a length scale representing the length of the region that is pyrolyzing or vaporizing and $y^* = (y/L)$ denotes the non-dimensional normal direction with reference to the surface that is issuing fuel vapor. k_w appearing in Eq.(1) is the thermal conductivity of the gas phase evaluated at the wall temperature and c_p is the specific heat measured at the adiabatic flame temperature of the given fuel. The term B that appears in Eq.(1) is a non-dimensional proportionality constant that relates the rate of mass transfer (e.g., vaporization, combustion) to the rate of heat transfer, and is essentially the driving force for mass transfer, and was first referred to as the "transfer number" by Spalding [4]. The Prandtl number, Pr, is assumed to be equal to unity. Eq.(1), thus, presents a convenient method to measure the local mass burning rates in such flames with high accuracy and ease. Knowledge of local pyrolysis rates in a solid fuel can be further used to calculate local heat fluxes and heat transfer coefficients in such flames.

3. Experimental Facility, Instrumentation and Uncertainty Analysis

The experimental facility includes a laboratory scale wind tunnel, fuel wick holder mounted atop a load cell and a set of thermocouples mounted on a 2-axis traverse mechanism. A 10 cm × 10 cm × 1.27 cm thick sheet of clear cast PMMA was used as a solid fuel sample, ignited by a propane torch. More details on the experimental setup can be found in the supplementary material of this manuscript and in literature elsewhere [3].

During experimental tests, the data acquisition system acquired temperatures at 500 samples per second, providing 500 samples to average per spatial point. Steady results were obtained for the first $150s$, when the surface remained relatively flat and transient results throughout the burning process. Reported temperatures are averages of at least five tests in a given condition and the maximum standard deviation was $< 3.2\%$ of the mean. The inherent uncertainty in temperatures measured by the thermocouple (T_{tc}) are taken to be 0.25% of the measured value based on manufacturer's specifications. The accuracy of the Nusselt number correlation used to calculate the radiation loss from the thermocouple bead was reported to be within 5% [5] and the uncertainty in k due to different species is assumed to be 3%. The error in the thermocouple emissivity (ε_{tc}) used is also small, $< \pm 3\%$, except that ε_{tc} is linear with T_{tc} so any error in T_{tc} increases the uncertainty in ε_{tc}. The Platinum emissivity was calculated using Jakob's theoretical correlation, confirmed by experimental data [6, 7] which reported the Pt emissivity uncertainty as $< \pm 3\%$ when using the calculation. The uncertainty in gas temperature is then calculated from a quadratic sum of the uncertainties,

$$dT_g = \left[\left(\frac{\partial T_g}{\partial T_{tc}} dT_{tc} \right)^2 + \left(\frac{\partial T_g}{\partial \varepsilon_{tc}} d\varepsilon_{tc} \right)^2 + \left(\frac{\partial T_g}{\partial k} dk \right)^2 + \left(\frac{\partial T_g}{\partial Nu} dNu \right)^2 \right]^{1/2} . \quad (2)$$

The maximum expanded uncertainty in gas temperatures is then found to be within ±14 K with a 95% confidence interval.

4. Results and Discussions

4.1. Steady Analysis of Local Mass Burning Rates and Wall Heat Fluxes in the Pyrolysis Zone

Figure 1 shows the variation of the local mass-burning rates for PMMA boundary layer diffusion flames along the streamwise length normalized by the fuel length, x^*, using the theoretical correlation from Eq.(1) and the non-dimensional temperature gradients at the condensed fuel surface. The local mass-burning rate evaluated by using Eq.(1) was also compared against the theoretical mass-burning rate given by Emmons [8] and is shown in Figure 1. The reasonably close agreement in estimating the local mass burning rates by using Eq.(1) and Emmons theoretical solution suggest that the proposed theoretical correlation works quite well in estimating the local mass burning rates for non-charring solid fuels.

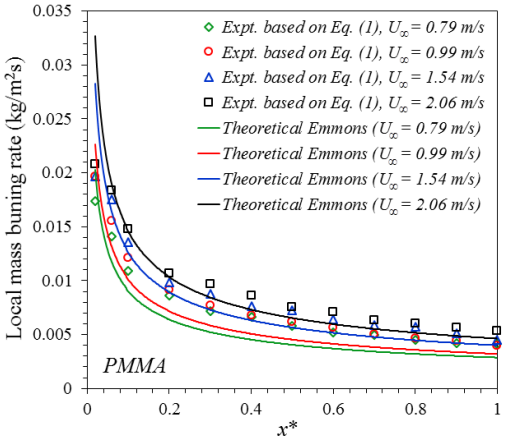

Figure 1: Variation of the local pyrolysis rates along the fuel surface for PMMA flames stabilized under different freestream conditions.

Utilizing gas-phase temperature measurements and local mass-burning rates, heat fluxes were evaluated in the pyrolysis zone at various stream-wise locations along the condensed fuel surface. Reasonable approximations were made to simplify the heat balance analysis and are discussed in literature elsewhere [2].

The energy balance at the condensed fuel surface ($y = 0$) for steady burning of solid fuels becomes [2],

$$\dot{m}''_f L_v = \dot{q}''_{fl,c} + \dot{q}''_{fl,r} - \dot{q}''_{s,rr} \tag{3}$$

and

$$\dot{m}''_f L_v = k_w \left(\frac{dT}{dy}\right)_{y=0} + \dot{q}''_{fl,r} - \sigma \left(T_w^4 - T_\infty^4\right), \tag{4}$$

where $\dot{q}''_{fl,c}$, $\dot{q}''_{fl,r}$, $\dot{q}''_{s,rr}$ and L_v represents the convective heat flux, radiative heat flux, re-radiation heat flux from the surface and effective heat of gasification or vaporization, respectively. Here, the convective heat flux is measured by using the expression $k_w \left(\partial T/\partial y\right)_{y=0}$ which represents the gas phase convective heating.

Re-radiation heat flux from the surface, $\dot{q}''_{s,rr}$, can be evaluated by knowledge of the wall and ambient temperatures, respectively. Utilizing Eq.(1), the net heat flux, $\dot{q}''_{net}$ ($\dot{q}''_{net}$=$\dot{m}''_f L_v$), can be estimated at various stream-wise locations along the pyrolysis zone simply by the knowledge of local mass burning rates along the condensed fuel surface. The effective heat of gasification or vaporization was taken to be 1.63 kJ/g for PMMA [9]. $\dot{q}''_{fl,r}$ can then easily be computed by using Eq.(4) above. The total heat flux incident to the surface, $\dot{q}''_{s,i}$, can be defined as the sum of the convective and radiative components of the flame heat flux. Figure 2 shows the various components of flame heat flux in the pyrolysis zone for PMMA boundary-layer diffusion flames stabilized at U_∞= 2.06 m/s.

Re-radiation from the PMMA surface was found to be significant when compared to liquid fuels. This is primarily due to increased surface temperatures in the case of PMMA (approximately 670±40 K). At a freestream velocity of U_∞ = 2.06 m/s, the average wall temperature for PMMA was measured to be 676 K. The total average incident heat flux to the wall was estimated to be 25.34 kW/m^2 while the average convective heat feedback from the flame to the wall was estimated to be 20.37 kW/m^2. The average radiative heat flux from the flame to the wall was then calculated to be 4.97 kW/m^2. Therefore, the radiative heat flux is 19.61% of the total incident heat flux for U_∞ = 2.06 m/s.

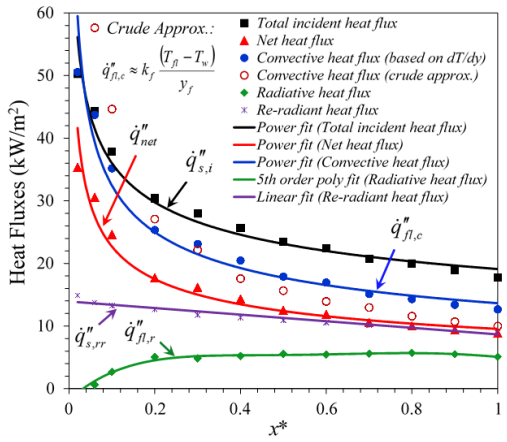

Figure 2: Variation of local heat flux profiles for a PMMA flame stabilized at U_∞= 2.06 m/s.

This radiative component is small because laminar flames are not sooty and do not radiate out a significant portion of the heat released, with the convective heat flux being the dominant mode of heat transfer. The average net heat flux, which is basically the sum of the convective and radiative heat fluxes minus reradiation from the surface, was then estimated to be 14.25 kW/m^2. It is to be noted that in the case of PMMA, the average net heat flux is quite lower than the total incident heat flux. This can be explained by the fact that a portion of the total incident flux is utilized in pyrolyzing the solid PMMA, whereas the rest is lost to the ambient surroundings through re-radiation from the solid wall. PMMA loses a considerable portion of total heat received by re-radiation compared to liquid fuels, owing to its higher surface temperatures.

The above results for PMMA flames suggest that convection is the dominant mode of heat transfer in steady laminar boundary-layer diffusion flames and is primarily responsible for the pyrolysis of fuel. Also, convective and total incident heat fluxes to the condensed fuel surface increases as the free-stream velocity increases. This results in higher burning rates at higher free-stream velocities.

4.2. Functional form of the Nusselt number

In this section, the relationship between local Nu_x and Reynolds number, Re_x, is presented. The effects of time-dependent processes on the burning rate of a PMMA plate in terms of local Nu_x and Reynolds number, Re_x is also presented.

Assuming Pr = 1, Emmons' exact solution for PMMA boundary layer diffusion flames stabilized under forced flow can be non-dimensionally expressed as,

$$\frac{\dot{m}''_f x}{\mu_\infty} = \left(\frac{\mathrm{Re}_x^{1/2}}{\sqrt{2}}\right) - f(0), \tag{5}$$

where $\mathrm{Re}_x = U_\infty x/\nu_\infty$ and ν_∞ is the kinematic viscosity at 300 K. $-f(0)$ is a function of the mass transfer number B and was approximated by Glassman [10] as,

$$-f(0) = \frac{\ln(1+B)}{2.6B^{0.15}}. \tag{6}$$

The convective heat feedback to the fuel surface at any x location, $h\Delta T$, can be approximated as $k\Delta T/y_f$, where h is the convective heat transfer coefficient, k is the gas-phase thermal conductivity, ΔT is the difference between the flame temperature and the wall temperature, $\Delta T = T_{fl} - T_w$, and y_f is the flame standoff distance. Therefore, the dimensionless Nusselt number can then be expressed in terms of normalized flame standoff distance (y_f/x) as, $\mathrm{Nu}_x = \frac{hx}{k} \approx \frac{x}{y_f}$. Local Nu_x at different streamwise locations along the condensed fuel surface can also be represented as,

$$\mathrm{Nu}_x = \frac{hx}{k_w} = \frac{h\Delta T x}{k_w \Delta T} \approx \frac{\dot{m}''_f L_v x}{k_w \Delta T}. \tag{7}$$

Neglecting radiation effects for small steady laminar boundary layer diffusion flames and considering pure convective heating in such flames, $h\Delta T$ is approximated as $\dot{m}''_f L_v$ in Eq.(7) above. Using Emmons' exact solution for $\dot{m}''_f$ and Glassman's approximation for $-f(0)$ in Eq.(7) above, Nu_x can finally be represented in a simplified form as,

$$\mathrm{Nu}_x = \left(\frac{L_v \mu_\infty}{k_w \Delta T}\right)\left(\frac{\mathrm{Re}_x^{1/2}}{\sqrt{2}}\right)\frac{\ln(1+B)}{2.6B^{0.15}}. \quad (8)$$

Using appropriate values for PMMA in Eq. (8) above, Nu_x can be expressed as

$$\mathrm{Nu}_x = 0.1148\sqrt{\mathrm{Re}_x}. \quad (9)$$

Table 1: Physical properties for evaluating Nu_x from Eq.(9).

Physical Properties	**PMMA**
Mass transfer number, B	1.3 [11]
Thermal conductivity, k_w (W/m-K) evaluated at the pyrolyzing wall temperature	0.050 [12]
Effective heat of vaporization, L_v (kJ/g)	1.63 [9]
$T_{fl,avg}$ (K) (present work)	1799
$T_{w,avg}$ (K) (present work)	672
ΔT (K) (present work)	1127
Dynamic viscosity, μ_∞ ($\times 10^{-6}$ Ns/m^2)	18.57 [12]

The transport properties used in the above expressions are given in Table 1. It is important to note that the average flame and wall temperature, obtained through experiments under different free-stream conditions, were used to calculate ΔT in Eq.(9) and that radiation was neglected in Eq.(9), therefore its application is limited to small steady laminar flames where gas phase convective heating is the dominant mode of heat transfer.

4.3. Normalized flame standoff distance

The normalized flame standoff distance, y_f/x can be expressed as the inverse of Nu_x for convectively-dominated boundary-layer diffusion flames (see Section 4.2). Figure 3 shows the normalized flame standoff distance versus $\sqrt{\mathrm{Re}_x}$. Experimental flame standoff distance was calculated by using the location of peak temperatures in such flames. The black line is Emmons' steady-state boundary layer solution and the symbols are the steady-state data points obtained

experimentally. The agreement of experimental data with the boundary layer predictions is quite good considering the approximations involved in deriving the theoretical Nu_x (normalized flame standoff distance, $y_f/x = 1/\mathrm{Nu}_x = 1/0.1148\sqrt{\mathrm{Re}_x}$). The slight departure of the experimental data from the Emmons' steady state boundary layer solution could be due to the uncertainties involved in the measurement of the flame standoff distance experimentally as well as due to the approximations involved in calculating Nu_x.

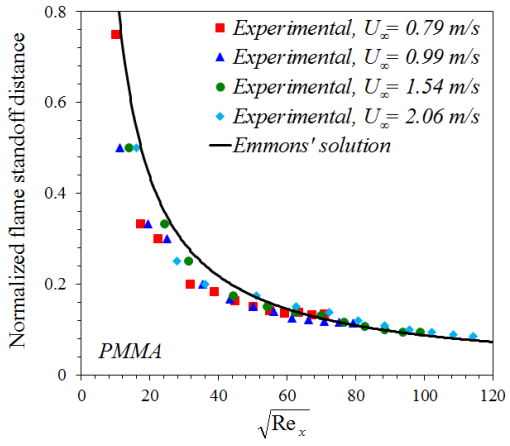

Figure 3: Normalized flame standoff distance versus $\sqrt{\mathrm{Re}_x}$ for PMMA boundary-layer diffusion flames under forced flow.

4.4. Steady local Nu_x for PMMA

Figure 4 shows the steady variation of Nu_x with $\sqrt{\mathrm{Re}_x}$ under free-stream velocities of 0.79, 0.99, 1.54 and 2.06 m/s. Emmons' steady-state boundary layer solution is obtained from Eq.(9) above, represented as a straight line in Figure 4. Experimental values for local Nu_x were calculated from the non-dimensional temperature gradients at the fuel surface [2],

$$\mathrm{Nu}_x = \frac{hx}{k_w} = +\frac{x}{L}\left(\frac{\partial T^*}{\partial y^*}\right)_{y^*=0}. \tag{10}$$

At low free-stream velocities, experimental data deviates slightly from the Emmons' steady-state boundary layer solution. However, good agreement was ob-

served between the experimental and theoretical data for higher free-stream velocities (U_∞= 1.54 and 2.06 m/s). As the velocity increases, the effects of buoyancy (namely lifting of the flame) decreases, thereby coming closer to Emmons' solution which neglects buoyancy.

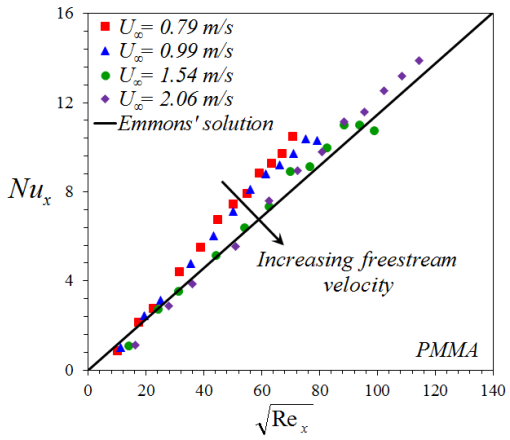

Figure 4: Local Nu_x versus $\sqrt{\mathrm{Re}_x}$ for PMMA boundary-layer diffusion flames under forced flow.

4.5. Transient local Nu_x for PMMA

For a PMMA burning surface, Nu_x can also be represented as [13],

$$\mathrm{Nu}_x = \frac{hx}{k_w} = \frac{R\rho_s L_v x}{k_w \Delta T}, \tag{11}$$

where R is the local regression rate, ρ_s is the PMMA solid density (1190 kg/m^3), L_v is the effective heat of gasification or vaporization, k_w is the gas-phase thermal conductivity evaluated at the wall temperature and ΔT ($\Delta T = T_{fl,avg} - T_{w,avg}$) is the difference between the average flame and wall temperature given in Table 1. Figures 5(a) and 5(b) show the variation of Nu_x with $\sqrt{\mathrm{Re}_x}$ for free-stream velocities of 0.79 and 2.06 m/s for test durations increasing from 100 to 850 s. The Emmons steady-state boundary layer solution for local Nusselt number is obtained as $\mathrm{Nu}_x = 0.1148\sqrt{\mathrm{Re}_x}$ and is the straight line shown in Figures 5(a) and (b).

At low $\sqrt{\mathrm{Re}_x}$ (the leading section), Figures 5(a) and (b) reveal that Nu_x decreases with time. This is seen in Figure 5(a) for $\sqrt{\mathrm{Re}_x} < 20$ and in Figure 5(b) for $\sqrt{\mathrm{Re}_x} < 30$. On the other hand, at large Re_x (downstream), the burning rate increases with time and transient effects are shown more clearly here. This is observed in Figure 5(a) for $\mathrm{Re}_x \geq 50$ and in Figure 5(b) for $\mathrm{Re}_x \geq 62$. At an intermediate Re_x, the burning rate is not transient and the data reveals a straight line trend (steady-state), which agrees well with the boundary layer solution. Near the leading edge (small Re_x) a gas phase steady state is attained within a short time after ignition, before a valley is formed. The close proximity of the flame to the fuel surface at the leading edge results in enhanced heat transfer rates (Fig. 2) which begin formation of this valley at short times. However, the burning rate soon starts decreasing as this valley forms because fuel-air mixing is retarded within this region. Thus, the burning rates in this section become smaller than the steady-state solution as time increases. Looking closely at Figure 5(a) for a free-stream velocity of 0.79 m/s, one can easily discern that for burn-out times of 100 and 150 s, the experimentally-measured Nu_x conforms to Emmons' steady-state solution. As the time progresses, the local burning rate in the leading section decreases while it increases in the trailing section.

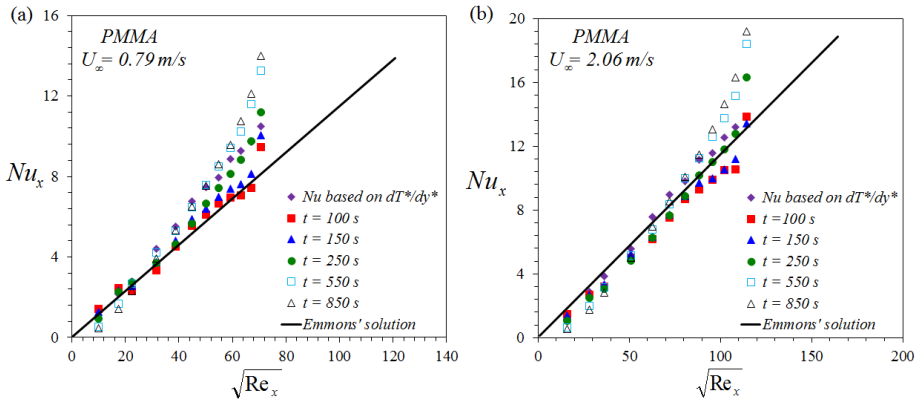

Figure 5: Transient Nu_x versus $\sqrt{\mathrm{Re}_x}$ for a PMMA boundary-layer diffusion flame stabilized at (a) (left) $U_\infty = 0.79$ m/s and (b) (right) $U_\infty = 2.06$ m/s, respectively.

In the trailing section, the gas phase also attains a steady state soon after uniform ignition and remains steady during the initial stages of burning ($t < 150$ s) when the PMMA surface is relatively flat. Non-uniform heating of the fuel surface (Fig. 2), however, causes varied surface regression which further modifies heat feedback as a function of time, especially at the leading and trailing ends of the sample. This leads to transient gas-phase heating effects at later times.

At higher burn-out times ($t > 150$ s) for a freestream velocity of 0.79 m/s, the experimentally measured Nu_x is large when compared to the steady-state boundary layer solution near the trailing edge ($\sqrt{\mathrm{Re}_x} > 50$). Similarly for a higher freestream velocity of 2.06 m/s, the experimentally measured Nu_x is large when compared to the steady-state boundary layer solution near the trailing edge ($\sqrt{\mathrm{Re}_x} > 80$) at higher burn-out times ($t > 250$ s). This clearly shows an increase in the burning rate of PMMA in the trailing section for longer burn-out times. At large Re_x (the trailing section) the heat feedback is small and it takes the sample considerable time to warm up and start pyrolyzing at a steady rate. Figures 5(a) and (b) show that at large U_∞, the warm up time is reduced and steady state is approached faster because of increased convection. For instance, looking at Figures 5(a) and (b), it can be clearly seen that at large Re_x (the trailing section), the experimentally measured Nu_x is large when compared to Emmon's steady-state solution for burn-out times higher than 150 s. At higher free-stream inlet velocities, the difference between the experimentally measured Nu_x and Emmon's steady-state solution becomes less for higher burn-out times ($t > 150s$).

The integrated mass loss rate for clear cast PMMA is known to increase with time thereby achieving a steady state at longer burn-out times. It was observed in our studies that the integrated mass burning rate for PMMA increases for longer burn-out times, however the increase in total mass burning rate was not found to be substantial. Interestingly, a compensatory mechanism was found to exist that kept the integrated mass burning rate of PMMA somewhat constant. Table 2 summarizes the variation of the integrated burning rate (BR) over the entire sample, in the leading section ($0 < x \leq 20$ mm), and over the rest of the

sample (20< x ≤100 mm), with time. Here the burning rate is obtained as $\sum R\rho_s \Delta x z$, where ρ_s is the PMMA solid density (1190 kg/m^3), R is the local regression rate, z is the sample width (0.1 m), Δx is a small increment in x associated with R, and the summation is between the limits of x. Table 2 shows that the integrated burning rate decreases with time in the leading section (as expected due to the formation of a valley), while it increases with time in the trailing section due to solid-phase heating. Table 2 indicates that the burning rate integrated over the entire plate does not vary much with time. Thus, the decrease in burning rate in the leading section seems to be compensated by the increase in the burning rate in the trailing section, confirming earlier observations made by Ndubizu et. al. [11] and should not be looked upon as a mere coincidence.

Table 2: Streamwise integrated burning rate (BR), total BR ($0 \leq x \leq 100$ mm), in the leading section ($0 < x \leq 20$ mm) and downstream ($x > 20$ mm) for a PMMA flame stabilized at a free-stream velocity of 2.06 m/s.

Free-stream velocity (m/s)	Test time (s)	Total BR entire surface (g/min)	BR (g/min) 0< x ≤20 mm	BR (g/min) 20< x ≤100 mm	% of total BR 0< x ≤20 mm	% of total BR 20< x ≤100 mm
2.06	100	4.67	1.78	2.88	38.15	61.85
2.06	150	4.68	1.77	2.91	37.87	62.13
2.06	250	4.65	1.57	3.08	33.67	66.33
2.06	550	4.77	1.35	3.42	28.21	71.79
2.06	850	4.75	1.22	3.53	25.66	74.34

Following the above observations, the transient pyrolysis behavior of a clear cast sheet of PMMA can be understood in more depth. After uniform ignition, the fuel surface starts to uniformly regress at a steady rate. Although the solid phase has not yet reached a thermal steady state, the gas phase achieves steady state behavior soon after ignition. This is because nearly all the incident heat feedback is used to gasify the solid at this stage. However, as time progresses, the incident heat flux decreases at the leading edge due to inefficient combustion, which can be attributed to slow removal of combustion products from the valley near the leading edge. It was also observed in our studies that the flame standoff

distance y_f increases with time (for $t > 150$ s) in the leading section (due to the formation of valley) but decreases with time (for $t > 150$ s) in the trailing section. No change in the flame standoff distance was observed for shorter burn-out times ($t < 150$ s). These moving boundary layer effects due to non-uniform surface regression along the length of the sample result in transient heat feedback to the surface at longer burn-out times. Following above observations, it can be concluded that heat feedback to the fuel surface decreases in the leading section while it increases in the trailing section for longer burn-out times ($t > 150$ s).

At shorter burn-out times, solid-phase pyrolysis can be assumed to be steady since it shows good agreement with Emmons' steady state solution both qualitatively and quantitatively. However, for longer burn-out times, the gas phase becomes highly transient due to formation of a valley in the leading section and therefore local pyrolysis rates for PMMA at a given streamwise location becomes transient. However, the solid phase now behaves in the exact opposite way, achieving steady state at longer burn-out times. For burning PMMA, any gas-phase measurements made at a later stage will not correspond to Emmons steady state boundary layer solution due to transient effects of the gas phase. These are important observations to keep in mind when assessing whether a fuel burns steadily just by using global mass-loss rates, as clearly spatial variations can arise which compensate for one another, complicating interpretation of these results.

5. Conclusions

A thorough experimental investigation was conducted on a bench scale experimental apparatus to identify the steady and transient burning regimes of a clear cast PMMA under forced flow. The results show that flames stabilized at higher freestream velocities conform closest to the Emmons' steady state solution. At lower freestream velocities, due to effects of buoyancy, experimental data was found to diverge from the Emmons' steady state solution. The results show that the agreement of the local mass burning rates is quite good with the

Emmons' steady state solution for low burn-out times. As time progresses and burn-out time increases, the local mass burning rate becomes transient and deviation from Emmons' steady state solution was observed. It is concluded in this work that gas phase measurements can only be compared with the Emmons' steady state solution at low burn-out times since during that time period heat incident upon the fuel surface is steady. As burn-out time increases, gas-phase measurements will not correspond to Emmons steady state boundary layer solution due to transient heat feedback to the fuel surface. A theoretical expression for the local Nu_x is derived in this work which can be readily used in both steady and transient applications.

References

[1] A. V. Singh, M. J. Gollner, Estimation of local mass burning rates for steady laminar boundary layer diffusion flames, Proceedings of the Combustion Institute 35 (3) (2015) 2527 – 2534. doi:10.1016/j.proci.2014.05.040.

[2] A. V. Singh, M. J. Gollner, A methodology for estimation of local heat fluxes in steady laminar boundary layer diffusion flames, Combustion and Flame 162 (5) (2015) 2214–2230. doi:doi:10.1016/j.combustflame.2015.01.019.

[3] A. V. Singh, M. J. Gollner, Local burning rates and heat flux for forced flow boundary-layer diffusion flames, AIAA Journal (2015) 1–11doi:10.2514/1.J054283.

[4] D. Spalding, Combustion of liquid fuel in gas stream, Fuel 29 (1) (1950) 2–7.

[5] D. Collis, M. Williams, Two-dimensional convection from heated wires at low reynolds numbers, Journal of Fluid Mechanics 6 (03) (1959) 357–384. doi:http://dx.doi.org/10.1017/S0022112059000696.

[6] L. M. Jakob, Heat Transfer: Vol. 1, Wiley, 1967.

[7] G. Gubareff, J. Janssen, R. Torborg, Thermal radiation properties survey, 1960, Minneapolis-Honeywell Regulator Company, Honeywell Research Center, Minneapolis.

[8] H. Emmons, The film combustion of liquid fuel, ZAMM-Journal of Applied Mathematics and Mechanics/Zeitschrift für Angewandte Mathematik und Mechanik 36 (1-2) (1956) 60–71. doi:10.1002/zamm.19560360105.

[9] J. G. Quintiere, Fundamentals of fire phenomena, John Wiley and Sons, England, 2006.

[10] I. Glassman, Combustion, Academic press, 1997.

[11] C. Ndubizu, R. Ananth, P. Tatem, Transient burning rate of a noncharring plate under a forced flow boundary layer flame, Combustion and flame 141 (1) (2005) 131–148. doi:doi:10.1016/j.combustflame.2004.12.013.

[12] S. Turns, An introduction to combustion, Vol. 287, McGraw-Hill New York, 1996.

[13] R. Ananth, C. C. Ndubizu, P. Tatem, Burning rate distributions for boundary layer flow combustion of a pmma plate in forced flow, Combustion and flame 135 (1) (2003) 35–55. doi:doi:10.1016/S0010-2180(03)00143-3.

Figure Captions

Figure 1. Variation of the local pyrolysis rates along the fuel surface for PMMA flames stabilized under different freestream conditions.

Figure 2. Variation of local heat flux profiles for a PMMA flame stabilized at U_∞= 2.06 m/s.

Figure 3. Normalized flame standoff distance versus $\sqrt{\mathrm{Re}_x}$ for PMMA boundary-layer diffusion flames under forced flow.

Figure 4. Local Nu_x versus $\sqrt{\mathrm{Re}_x}$ for PMMA boundary-layer diffusion flames under forced flow.

Figure 5. Transient Nu_x versus $\sqrt{\mathrm{Re}_x}$ for a PMMA boundary-layer diffusion flame stabilized at (a) (left) U_∞ = 0.79 m/s and (b) (right) U_∞ = 2.06 m/s, respectively.

Tables

Table 1. Physical properties for evaluating $\mathbf{Nu}_x$ from Eq.(9).

Table 2. Streamwise integrated burning rate (BR), total BR ($0 \leq x \leq 100$ mm), in the leading section ($0 < x \leq 20$ mm) and downstream ($x > 20$ mm) for a PMMA flame stabilized at a free-stream velocity of 2.06 m/s.